

Observations of Barrier Layer Seasonal Variation in the Banda Sea

M. F. A. Ismail^{1,2}, J. Karstensen¹, A. Sulaiman², B. Priyono², A. Budiman², A. Basit², A. Purwandana², T. Arifin².

¹GEOMAR Helmholtz Centre for Ocean Research Kiel, Kiel 24148, Germany.

²National Research and Innovation Agency of Indonesia, Jakarta 10340, Indonesia.

Corresponding author: Mochamad Ismail (fismail@geomar.de)

Key Points:

- First study estimating barrier layer thickness (BLT) in the Banda Sea using comprehensive observations
- A quasi-permanent barrier layer exists in the Banda Sea with seasonal variation in occurrence and thickness
- The horizontal intrusion of low saline waters and anticyclonic circulation are identified as the main mechanisms for creating and modulating the local BLT

17 **Abstract**

18 The Banda Sea is of crucial importance for the circulation of the world's oceans, as it is part of
19 the connection between the Pacific to the Indian Ocean. One peculiarity of the upper ocean
20 hydrography in the Banda Sea is the occurrence of barrier layers. The regionality and temporal
21 variability of barrier layer thickness (BLT) in the Banda Sea are examined in this study utilizing
22 in-situ observations and ocean reanalysis output. It is found that a barrier layer occurs in over 90
23 % of the observational data profiles, and in over 72 % of those profiles, the BLT is shallower
24 than 10 m. Furthermore, we find a seasonal cycle in BLT with a maximum thickness of about 60
25 m occurring during austral autumn and winter and coinciding with the presence of low saline
26 waters fed by the regional river discharge and rainfall from the Java Sea and Makassar Strait. In
27 addition, we identify the existence of a quasi-permanent anticyclonic circulation cell in the
28 Banda Sea that may support the trapping of surface freshwater by retention. The anticyclonic
29 circulation is most likely wind-driven because it coincides with the regional Ekman pumping
30 pattern. Modulation of the anticyclone is via seasonal variability in the wind stress curl which in
31 turn may explain the efficiency of freshwater retention and thus the BLT. The annual mean BLT
32 distribution in the Banda Sea shows a preferential region of thickened barrier layers around 6°-
33 8°S and 124°-126°E and resampling the pattern of the monthly mean climatology.

34

35 **Plain Language Summary**

36 The Banda Sea is crucial to the circulation of the world's oceans and atmosphere due to its
37 location within the equatorial regions of the Indonesian Maritime Continent. It links the Pacific
38 and Indian Oceans' circulation via the Indonesian Throughflow and contributes to driving
39 atmospheric conditions via heat and moisture fluxes. Strong salinity-stratified barrier layers
40 insulate the water exchange between the surface and subsurface. The formation and seasonal
41 variation of barrier layer thickness (BLT) in the Banda Sea are analyzed based on all available
42 observations and ocean reanalysis outputs. Observations show that the Banda Sea has a barrier
43 layer for the most part of the season. The BLT maximum appears during austral winter (June to
44 August) months. The seasonal BLT maximum is attributed to the near-surface water freshening,
45 which shoals the mixed layer depth (MLD) and deep isothermal layer depth (ILD) maintained by
46 a steady anticyclonic gyre. Other processes, such as wind stress curl-induced Ekman pumping
47 associated convergence, also modulate its seasonal variability.

48

49

50

51

52

53

54

55 **1 Introduction**

56 A surface mixed layer with vertically quasi-homogenous properties in temperature and
57 salinity exists over a large part of the global ocean (de Boyer Montégut et al. 2004). A region
58 with a strong density gradient, the pycnocline, generally marks the base of the mixed layer. Air-
59 sea interactions permanently modify mixed layer properties, and the downward propagation of
60 properties from the air/sea interface is due to a complex interaction of buoyancy (composed of
61 heat and freshwater forcing) and momentum fluxes mediated by mixing processes. In tropical
62 oceans, the seasonality of heat flux is less pronounced compared to the subtropical or the high
63 latitude ocean. However, one phenomenon that is well developed over parts of the tropical ocean
64 is the formation of barrier layers (Lukas & Lindstrom, 1991; Sprintall & Tomczak, 1992). A
65 freshwater surplus at the ocean surface, either from rainfall or riverine sources, can create its
66 own, and sometimes very local, density gradient within an otherwise rather homogenous in
67 temperature (and density) layer. This way the low salinity-driven mixed layer depth (MLD) can
68 be shallower than a temperature-defined isothermal layer depth (ILD) that characterizes more the
69 background mixed layer. A layer difference between the MLD and deeper ILD is referred to as
70 the barrier layer because it acts as a barrier against the vertical exchange of heat, salt, and
71 momentum between the near-surface and the top of the thermocline (Drushka et al., 2014; Kara
72 et al., 2003; Katsura et al., 2022). Lukas and Lindstrom (1991) were the first to study the barrier
73 layer in the Western Equatorial Pacific and found it linked to local buoyancy gain of the ocean
74 surface by heavy precipitation. Barrier layers have attracted increasing research interest and have
75 been documented globally (de Boyer Montégut et al., 2007) in many regional oceans, such as in
76 the Arabian Sea (e.g., Thadathil et al., 2008), the Bay of Bengal (e.g., Kumari et al., 2018), the
77 Indo-Australian Basin (e.g., Qu & Meyers, 2005), and the South China Sea (e.g., Liang et al.,
78 2018).

79

80 The development of barrier layers involves various physical mechanisms that regulate the
81 ILD and MLD, including wind-driven downwelling (e.g., Pang et al., 2019), horizontal advection
82 of low salinity waters (e.g., George et al., 2019), net freshwater fluxes (e.g., Katsura et al., 2022),
83 and relative vorticity (e.g., d'Ovidio et al., 2013). It is suggested that barrier layer thickness
84 (BLT) extends from several meters to a hundred meters and varies temporally and spatially
85 (Mignot et al., 2007; de Boyer Montégut et al., 2007). The existence of barrier layers has
86 substantial thermodynamic and dynamic implications. It is found that barrier layers in tropical
87 oceans limit the upward intrusion of cold thermocline water into the mixed layer, trap heat in the
88 mixed layer, and lessen the impacts of atmospheric heat forcing on the mixed layer (Drushka et
89 al., 2014; Katsura et al., 2022). Both processes enhance regional surface temperature anomalies
90 and elevate atmospheric convection (Ivanova et al., 2021; Li et al., 2017). The evolution of BLT
91 influences air-sea exchange on time scales ranging from sub-seasonal (Pujiana & McPhaden,
92 2018) to seasonal time scales (Felton et al., 2014). Early research has shown the barrier layer's
93 impact on large-scale ocean-atmosphere interactions in the Indian Ocean (Drushka et al., 2014;
94 Kumari et al., 2018) and the Pacific Ocean (Corbett et al., 2017; Maes et al., 2005). Using an
95 observational and coupled ocean-atmosphere model, Maes et al. (2005) demonstrated the
96 significant role of barrier layers in maintaining anomalous warm water over the equatorial
97 eastern Pacific, ultimately promoting the formation of El Niño Southern Oscillation (ENSO). In
98 the Indian Ocean, Qiu et al. (2012) highlighted a robust link between barrier layer variability and
99 the formation of the Indian Ocean Dipole (IOD). Further, they suggested that an IOD-induced

100 co-varying barrier layer improves the IOD positive feedback. A recent study by Ivanova et al.
101 (2021) has shown that the variability of BLT in the East Indian Ocean strongly correlates with
102 the rainfall over West Sumatra and Australia. Further, Ivanova et al. (2021) argued that barrier
103 layers might be used to predict intensified rainfall over northern Australia. The preceding studies
104 highlight the significant role of barrier layers in controlling ocean-atmosphere interactions,
105 which impact weather and climate.

106

107 The Banda Sea (Fig. 1a) is the largest tropical semi-enclosed sea in the Indonesian
108 Maritime Continent (IMC). Due to its unique location, the Banda Sea is essential to the
109 circulation of the world's oceans and atmosphere (Gordon et al., 1994; Lee et al., 2019; Wang et
110 al., 2023; Yin et al., 2023; Yoneyama & Zhang, 2020; Yuan et al., 2022). It connects the tropical
111 Pacific and Indian Oceans' circulation via the Indonesian Throughflow and contributes to
112 regional climate through heat, salt, and momentum fluxes (Atmadipoera et al., 2022; Jochum &
113 Potemra, 2008; Yin et al., 2023; Yuan et al., 2022). At intraseasonal time scales, the Banda Sea
114 sea surface temperature (SST) is modulated by the Madden-Julian Oscillation (MJO; Napitu et
115 al., 2015; Pei et al., 2021). The upper ocean circulation in the Banda Sea is controlled by
116 seasonally reversing monsoonal winds from the northwest during the austral summer and from
117 the southeast during the austral winter (Gordon & Susanto, 2001; Ilahude & Gordon, 1996;
118 Ismail et al., 2023; Kida et al., 2019; Sprintall & Liu, 2005; Zhu et al., 2019). The southeast
119 monsoon drives basin-wide wind-induced mixing (Thomas et al., 2003), strong outflow through
120 the Timor Passage and into the Indian Ocean (Kida et al., 2019), and quasi-stationary
121 anticyclonic eddy in the southwest boundary of the Banda Sea (Liang et al., 2019; Zhu et al.,
122 2019). In contrast, the northwest monsoon current carries low salinity water from the Java Sea
123 and Makassar Strait through rainfall and river discharge (Halkides et al., 2011; Ilahude &
124 Gordon, 1996; Kida et al., 2019; Zhu et al., 2019). This freshwater influx, which has a
125 pronounced low sea surface salinity signature (< 34), is overlying saline subsurface water and
126 creates a strong salinity stratification in the Banda Sea that is forming a regional barrier layer
127 (Ismail et al., 2023).

128

129 Barrier layers in the eastern Indian Ocean and west of the IMC have been suggested to
130 warm the upper ocean and in turn intensify the rainfall in Australia and Indonesia (Ivanova et al.,
131 2021). So far, little attention has been given to the drivers and variability of the barrier layer in
132 the Banda Sea. Ismail et al. (2023) used data from a single Argo float from the eastern Banda Sea
133 to document the temporal evolution of salinity stratification and barrier layer thickness. Here, we
134 extend the earlier study and examine the spatial distribution and variation of barrier layers in the
135 Banda Sea. We also consider the physical processes that support and maintain their formation
136 and bridge this information with the local climate forcing. We make use of all available historical
137 observations data from multiple platforms (i.e., conductivity-temperature-salinity-depth (CTD)
138 instruments and Argo floats) and also consider data from an ocean reanalysis model.

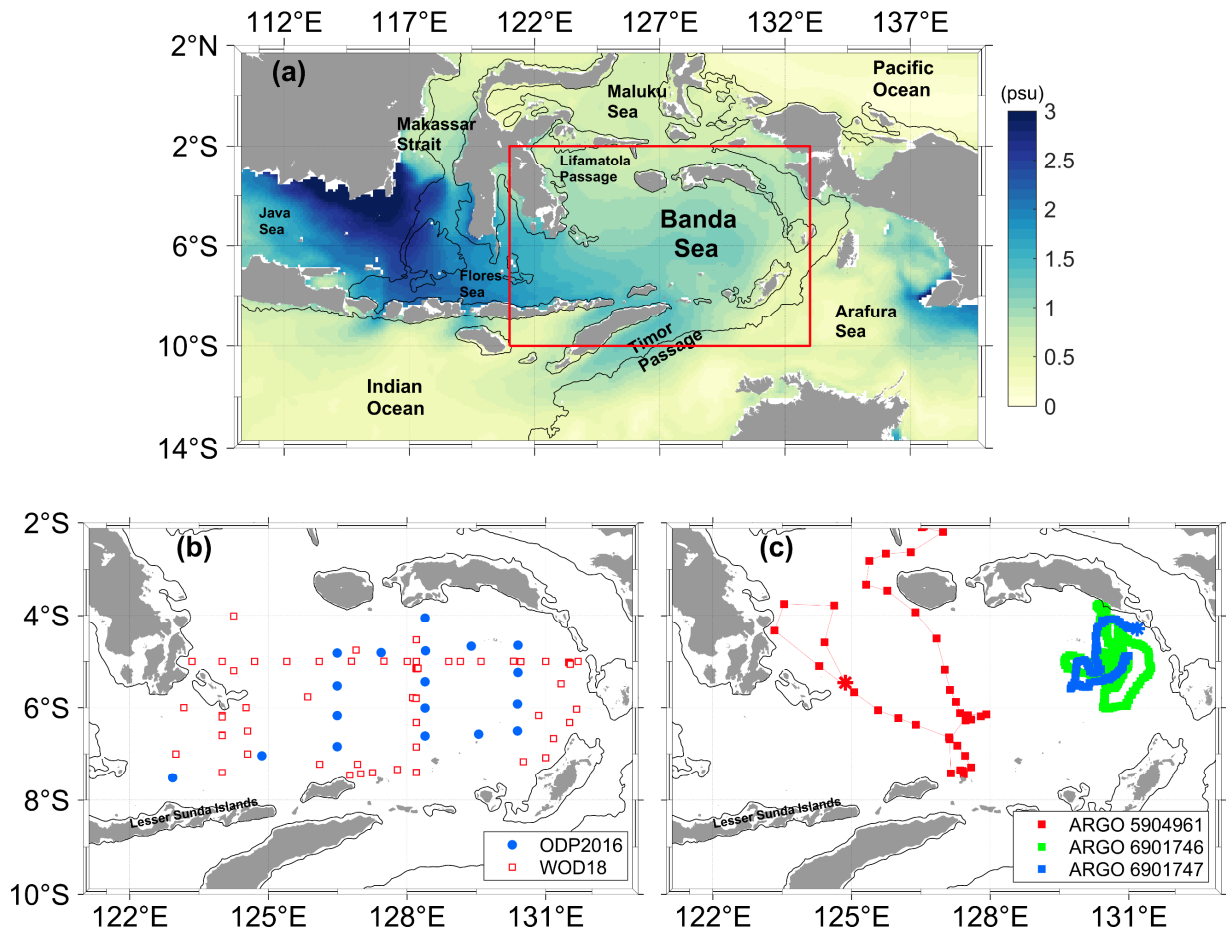
139

140 **2 Materials and Methods**

141 2.1 Observational data

142 The historical CTD data used in this study originates from the Ocean Dynamics Program
 143 for the Banda Sea (ODP2016) and several research field campaigns archived in the World Ocean
 144 Database 2018 (WOD18) and include the International Oceanographic Data and Information
 145 Exchange project and NOAA National Center for Environmental Information (Boyer et al.,
 146 2018). The ODP2016 cruise (Fig. 1b) consisted of 18 CTD profiles (upper 1,000 m) of
 147 temperature and salinity measured using the SBE 911+ system onboard the *RV Baruna Jaya VIII*
 148 between 29 August and 5 September 2016 (Table 1). The WOD18 data consists of 80 CTD
 149 profiles collected between 1993 and 2001 (Fig. 1b and Table 1). CTD data from three Argo
 150 floats (WMO ID: 5904961, 6901746, and 6901747) are also used (Fig. 1c).

151



152

153 **Figure 1.** (a) Geographic features of the Indonesian Seas overlaid with the magnitude of the
 154 seasonal cycle in salinity from January 1993 - December 2022 based on BRAN2020. (b)
 155 Positions of CTD stations of the Ocean Dynamics Program for the Banda Sea (ODP2016) and
 156 stations archived in the World Ocean Database 2018 (WOD2018). (c) CTD profile positions
 157 (squares) and trajectories (lines) of Argo floats 5904961, 6901746, and 6901747. The red

158 rectangle in **(a)** outlined the location of the area captured in **(b)** and **(c)**. The red, green, and blue
159 asterisk in **(c)** denotes the end location of Argo floats 5904961, 6901746, and 6901747,
160 respectively. The solid black lines in a, b, and c denote the 500 m isobath.

161

162 2.2 Ocean and atmosphere reanalysis products

163 The gridded data from the Bluelink ReANalysis version 2020 (BRAN2020) model is
164 used to investigate the BLT seasonal climatology from January 1993 to December 2022 and to
165 add to the individual CTD station's observational data a coherent time/space context.
166 BRAN2020 is based on the global eddy-resolving Ocean Forecasting Australia Model (OFAM3)
167 released in May 2021 (Chamberlain et al., 2021; Oke et al., 2013; Schiller et al., 2020). A
168 complete description of OFAM3 is provided by Oke et al. (2013). The model has $1/12^\circ$
169 horizontal resolution for all longitudes, between latitude 75°S to 75°N , and 51 vertical levels with
170 5 m vertical resolution down to 40 m, 10 m vertical resolution from 40 m to 200 m, and 500 m
171 thick below 2000 m. BRAN2020 outputs realistically produce the ocean circulation and perform
172 comparatively well compared to Argo floats observations in the Banda Sea (Fig. S1 to S3). It
173 shall be noted that Argo float data we use for our analysis is also assimilated in the BRAN2020.
174 A recently published study evaluating three global ocean reanalysis products demonstrates that
175 BRAN2020 outperforms the Hybrid Coordinate Ocean Model and Mercator Ocean's Global
176 Reanalysis in Southern Africa, especially for the MLD (Russo et al., 2022). Numerous
177 researches in the Australasian region have been supported by BRAN2020 data, including
178 analysis of the Fraser Gyre off southeast Queensland (Ismail et al., 2017), studies of
179 intraseasonal variability of the ITF (Schiller et al., 2010), and mixed layer heat and mass budget
180 in the Banda Sea (Ismail et al., 2023). Near-surface zonal and meridional wind data for the
181 period January 1993 to December 2022 from the fifth generation (ERA5) of the global climate
182 and weather outputs of the European Center for Medium-Range Weather Forecasts (Hersbach et
183 al., 2023) were also used in this study.

184

185 2.3 Determining ILD, MLD, BLT, and relative vorticity

186 The ILD and MLD are computed according to the de Boyer Montégut et al. (2004) and
187 Holte and Talley (2009) algorithms. The ILD is computed as the interpolated depth where the
188 temperature ($^\circ\text{C}$) has decreased by 0.2°C from the reference depth of 10 m. The reference depth
189 of 10 m is utilized to eliminate the diurnal variations of ocean surface water at the first few
190 meters (Breugem et al., 2008). The MLD is computed as the interpolated depth at which
191 potential density (σ_θ) increases from the reference depth (10 m) by the equivalent value of 0.03
192 kg m^{-3} . The BLT is the positive difference between the ILD and MLD with at least 2 m in
193 magnitude.

194

195 From BRAN2020, we compute the relative vorticity ζ (s^{-1}) to characterize the ocean's
196 local rotational flow (Rudnick et al., 2019) and as an indicator of mesoscale processes that may
197 be linked to the distribution of BLT in the Banda Sea. The relative vorticity is computed as
198 follows:

$$\zeta = \frac{\partial v}{\partial x} - \frac{\partial u}{\partial y} \quad (1)$$

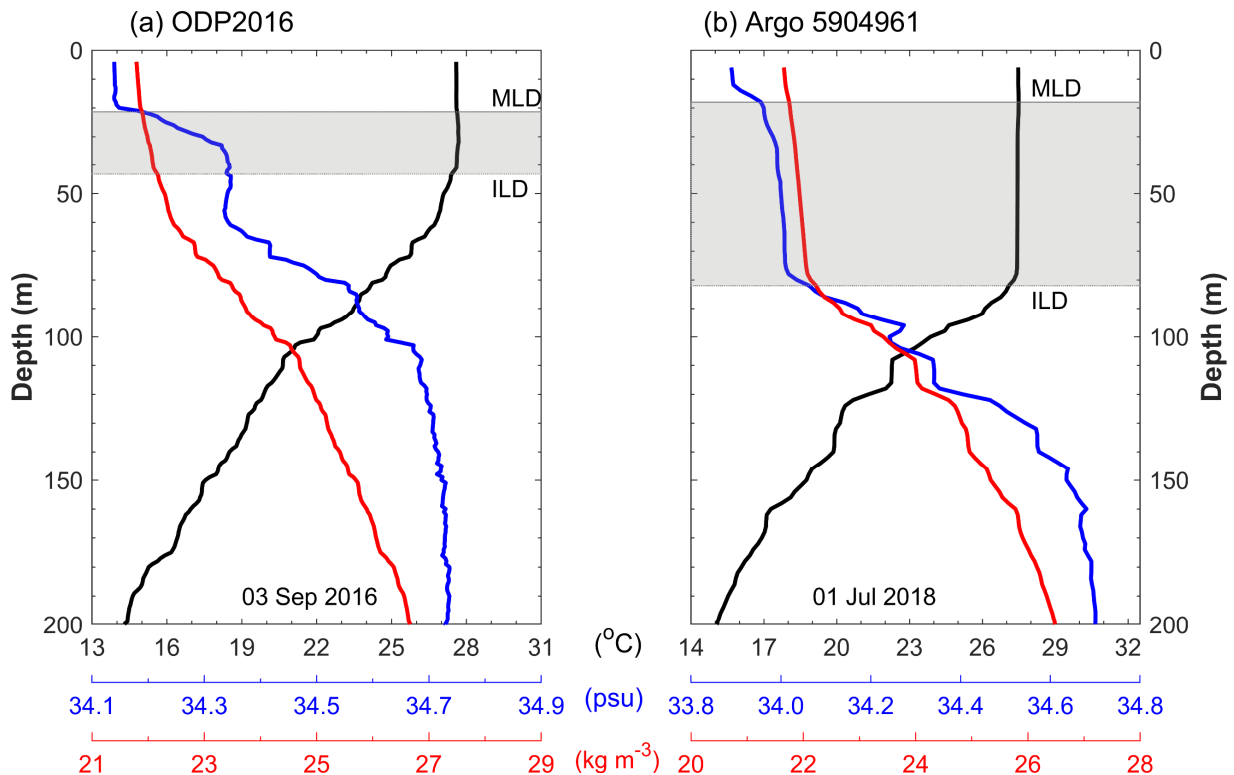
Where u and v are zonal and meridional velocity (m s^{-1}) from BRAN2020, and x and y are zonal and meridional position. Positive and negative relative vorticity represent anticyclonic and cyclonic mesoscale features.

3 Results and Discussion

3.1 Evidence of the barrier layer from observations

As example, Figure 2 show selected temperature, salinity, and density profiles over the upper 200-m from ODP2016 and Argo 5904961 in the Banda Sea. The respective ILD, MLD, and BLT are indicated. For both profiles, the halocline aligns well with the pycnocline. Moreover, the upper thermocline layers that mark the ILD are about 50 m (80 m) deep in ODP2016 (Argo 5904961), with large vertical fluctuation between the 14°C and 28°C isotherms. While temperature tends to be nearly homogenous from the surface to the upper thermocline layer, salinity increases from approximately 34.15 to 34.40 (33.90 to 34.20) from about 20 m to 40 m (20 m to 80 m) depth (Fig. 2). This salinity increase causes a shallow density gradient near a depth of about 20 m and inside the ILD. Figures 2a and 2b also reveal that pycnoclines in the Banda Sea are likely determined by salinity. A halocline above the thermocline leads to the MLD becoming shallower than the ILD, indicating the existence of a barrier layer. The MLD on 03 September 2016 is about 20 m. Below it is a barrier layer about 21 m thick (Fig. 2a). Similar shallower MLD was also observed on 01 July 2018, albeit the barrier layer is thicker, exceeding 60 m (Fig. 2b).

The barrier layer occurrence distributions have been observed for more than 90 % of all profiles (Table 1) in the Banda Sea. For example, among 18 CTD stations during the ODP2016 cruise, there are 17 stations where the barrier layer occurs. Thus, the rate of occurrence reaches 94.44 %, though most of the BLT is under 9 meters. Table 1 shows two groups of CTD data with high occurrence rates of BLT in the Banda Sea. They were observed from 12 to 13 November 1995 and 28 February to 4 March 1998. These BLT have a mean value ranging from 2.30 m to 13.57 m (see Table 1). To explore the spatial distribution of BLT in the Banda Sea, we computed all observation profiles and projected them into a geographical map (Fig. 3a). The results denote that BLT is generally shallow, with about 72 % of profiles having BLT less than 10 m. BLT deeper than 30 m are predominantly obtained from Argo profiles along its trajectories. To further analyze BLT distribution from all observations, we computed the probability density function (PDF) (Fig. 3b). It appears that high BLT densities are in the range of 2-10 m, which is in line with BLT spatial distribution (Fig. 3a). In addition, the PDF is highly skewed toward an increase of BLT values.



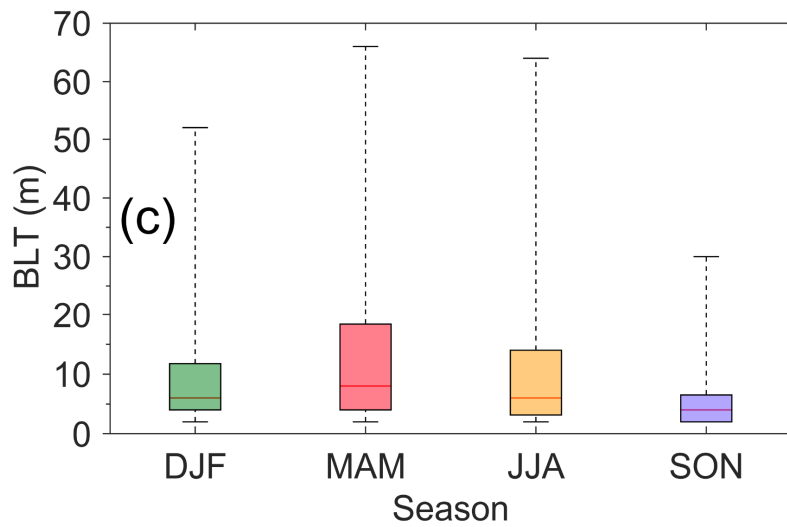
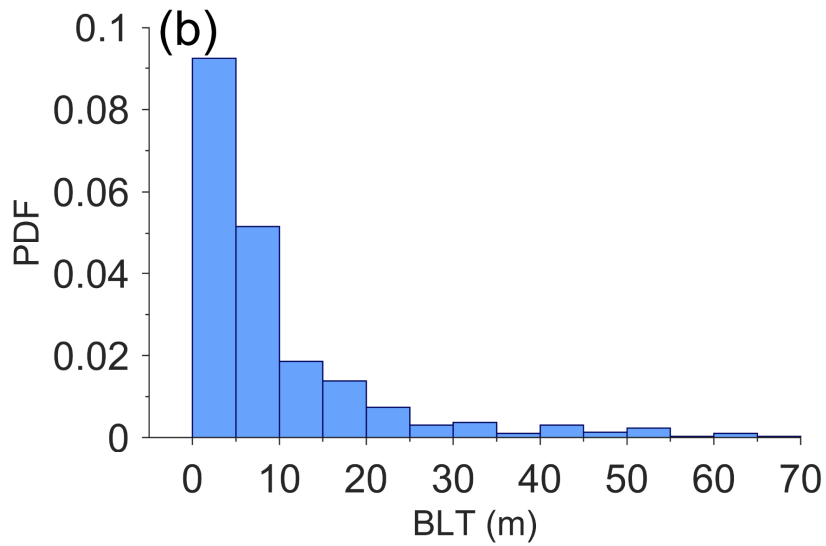
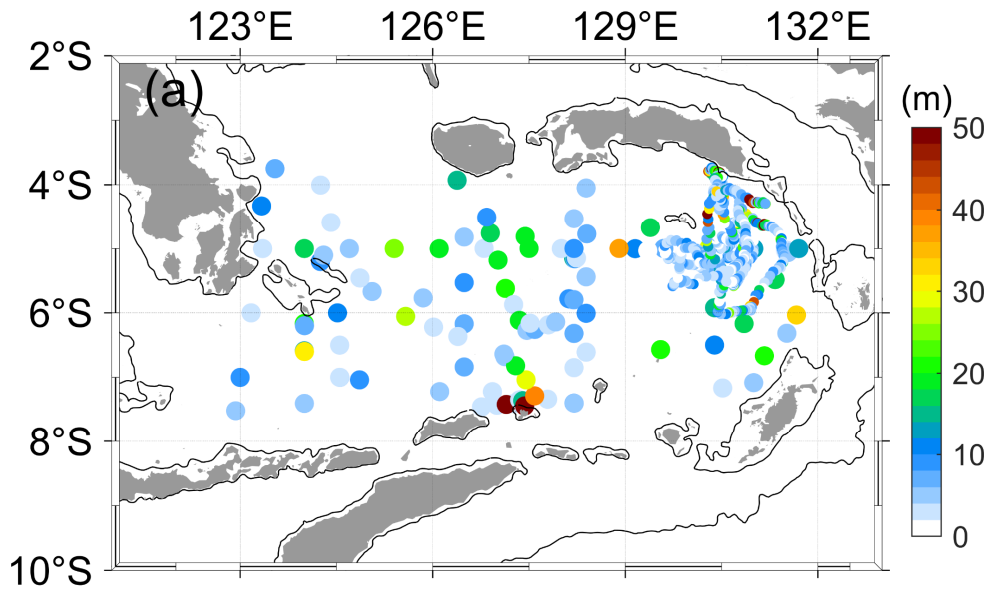
236

237 **Figure 2.** Vertical profiles of temperature ($^{\circ}\text{C}$; black line), salinity (psu ; blue line), and density (kg m^{-3} ; red line) in the Banda Sea from (a) ODP2016 on 3 September 2016, and (b) Argo 5904961
 238 on 1 July 2018. The grey lines denote the MLD, and the dashed grey lines represent the ILD. The
 239 grey-shaded area is the section of the water column termed BLT.
 240

241

242 To assess the seasonal variation of BLT from observations in the Banda Sea, we
 243 quantified the statistical values of the BLT in each season shown in Fig. 3c. The available data
 244 acquired during different seasons and years allow us to estimate a seasonal cycle i.e., December
 245 to February (DJF) represents austral summer, March to May (MAM) illustrates austral autumn,
 246 June to August (JJA) defines austral winter, and September to November (SON) represents
 247 austral spring. The analysis shows that the barrier layer was found to be thicker in MAM and JJA
 248 than in SON and DJF. The seasonality of BLT was highly significant, with p values < 0.001 . The
 249 thick barrier layer during MAM (JJA) exhibited a median value of 8.0 m (6.0 m) with upper
 250 quartiles above 13 m depth. The maximum value of BLT during MAM and JJA reached 66 m
 251 and 64 m, respectively. Those maximum values were obtained from Argo 6901746 and Argo
 252 5904961, respectively. In contrast, thin barrier layers are found in SON. The median of BLT
 253 during DJF and SON is 6 m and 4 m, respectively, with both upper quartiles below 13 m. During
 254 DJF (SON), it is observed that the highest value of BLT reaches at most 52 m (30 m). The
 255 statistical analysis above suggests that the estimated BLT from observations in the Banda Sea
 256 has an apparent seasonal variation, with BLT maximum and minimum observed in MAM and
 257 SON, respectively.

258



260 **Figure 3.** (a) Spatial distribution, (b) probability density distribution (%), and (c) box-whisker
 261 plots of BLT (m) estimated from all observations in the Banda Sea. The boxes in (c) are defined
 262 by lower and upper quartiles, and the center red lines in the boxes represent the median, caps at
 263 the end of the boxes exhibit minimum and maximum values. The solid black lines in a show the
 264 500 m isobaths.

265

266 The source of the upper layer water masses entering the Banda is identified using
 267 potential temperature-salinity (T-S) diagrams (Fig. 4). The T-S diagrams showed that fresher (<
 268 34) and relatively warm (> 27°C) water masses within σ_θ values range of 20 – 22 kg m⁻³
 269 observed almost in all season in the Banda Sea, except during the SON. Previous studies
 270 identified this surface water as Java Surface Water (JSW). JSW is characterized by a
 271 homogenous salinity below 34, potential temperature between 27°C - 30°C, and σ_θ values below
 272 22.00 kg m⁻³ (Atmadipoera et al., 2022; Ilahude & Gordon, 1996; Kida et al., 2019). Kida et al.
 273 (2019) demonstrated that the source of the JSW is intense net precipitation during DJF in the
 274 Java Sea. In the Banda Sea, JSW first appeared during DJF (Fig. 4a) and reached its peak
 275 occurrence during MAM (Fig. 4b). During JJA the JSW presence declines (Fig. 4c) while during
 276 SON it is not observed in the Banda Sea (Fig. 4d). The presence of JSW in the Banda Sea during
 277 DJF, MAM, and JJA indicated direct intrusion of the regional river discharge and rainfall from
 278 the Java Sea and Makassar Strait (see Fig. 1a). Through applying a particle tracking model, Kida
 279 et al. (2019) suggested that the JSW remains and accumulated near the surface of Banda Sea
 280 from DJF to MAM before exiting through the Timor Passage in SON. The existence of JSW in
 281 the Banda Sea caused a decrease in salinity, which later induced a shallower MLD compared to
 282 ILL, thus thickening the barrier layer in the Banda Sea.

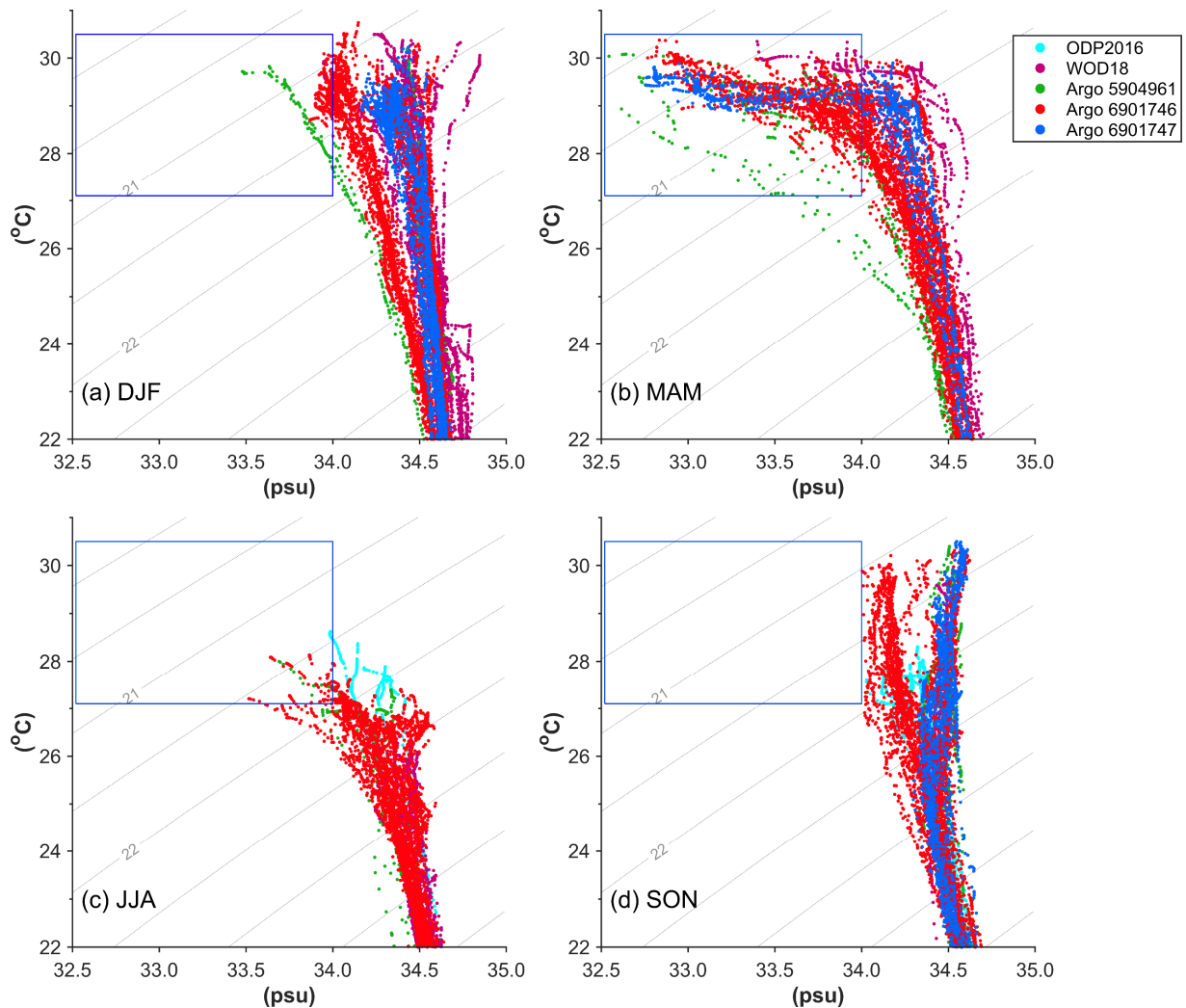
283

284 **Table 1.** General statistics of the observed barrier layer in the Banda Sea.

Source	Observation Periods	Number of profiles	% Occurrence of BLT > 2 m	Mean BLT (m)
ODP2016	29 Aug 2016 – 5 Sep 2016	18	94.44	9.05
	29 Jul 1992 – 4 Aug 1992	10	90.00	11.57
	29 Aug 1993 – 3 Sep 1993	15	93.33	8.50
WOD18	31 Jan 1994 – 09 Feb 1994	17	94.12	7.91
	12 Nov 1995 – 13 Nov 1995	5	100.00	2.30
	04 Dec 1996 – 13 Dec 1996	17	94.12	4.12
	28 Feb 1998 – 4 Mar 1998	16	100.00	13.57
Argo 5904961	23 Jun 2018 – 8 Dec 2018	31	97.77	13.42
Argo 6901746	29 Jul 2017 – 28 Aug 2019	414	90.09	9.17
Argo 6901747	4 Sep 2018 – 7 Apr 2019	109	89.91	9.67

285

286



287

288 **Figure 4.** Potential temperature ($^{\circ}\text{C}$) versus salinity diagram in the upper ocean layer for (a)
 289 December to February (DJF), (b) March to May (MAM), (c) June to August (JJA), and (d)
 290 September to November (SON) obtained from all observations in the Banda Sea (Fig. 1b and c).
 291 The grey contours with numbers show isopycnic lines. The blue rectangle indicates the
 292 characteristics of JSW.

293

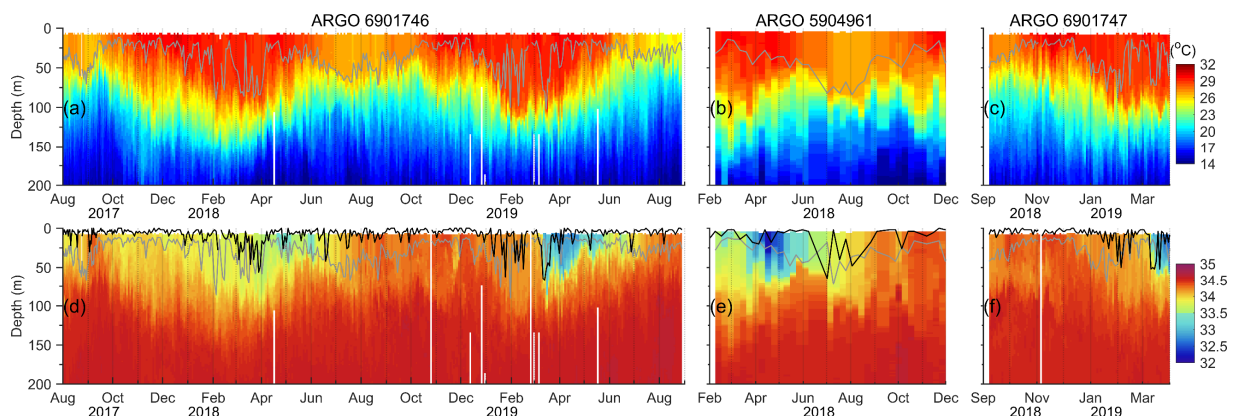
294 The time series of the barrier layer derived from temperature and salinity profiles from all
 295 available three Argo floats in the Banda Sea is shown in Figure 5. In general, the vertical
 296 temperature in the upper 150 m shows seasonal temperature increase reaching above 29°C from
 297 DJF to early MAM, after which they decrease to below 26°C during JJA (Fig. 5a-5c). The
 298 seasonal buildup of near-surface warm (cold) waters during DJF (JJA) is a distinct feature of the
 299 Banda Sea (Gordon & Susanto, 2001; Ismail et al., 2023). The 29°C (26°C) isotherm during DJF
 300 (JJA) extends to about 100 m (70 m) depth, which marks the base of the ILD. Below the ILD, the
 301 thermocline exists in which the temperature reduces significantly by 15°C over a depth range of

302 about 100 m. The thermocline layer average position exhibits significant upward and downward
 303 movement on seasonal time scales in phase with the ILD. The first maxima of the thermocline
 304 layer occur mainly during DJF and the second maxima during JJA. Like the thermocline
 305 variability, the ILD from Argo 6901746 (eastern Banda Sea) shows seasonal variability with a
 306 bimodal distribution. The first maxima of about 90-100 m deep, was observed during late DJF
 307 and the second maxima reached up to 70 m deep during JJA (Fig. 5a). Because both cover only
 308 one season, Argo 5904961 and 6901747 captured only one peak of deeper ILD in JJA and DJF,
 309 respectively (Fig. 5b-5c). Following Argo 6901746, the ILD maximum from Argo 5904961
 310 (6901747) also appeared in JJA (DJF to early MAM), reaching up to 80 m.

311

312 Like the temperature, the time-depth salinity profiles show seasonal variations in the
 313 upper 100 m depth (Fig. 5). The salinity structures of the upper layers during the observational
 314 period of Argo float 6901746, covering roughly two years, also show two freshening events (Fig.
 315 5), while Argo floats 5904961 and 6901747 both show only one freshening event, due to their
 316 shorter (less than a year) deployment time, but well synchronized with Argo 6901746. The
 317 freshening events are characterized by relatively low saline water ranging from 32.0 to 34.0 in
 318 the upper 70 m, mainly observed from February to June. Moreover, for Argo 6901746 the near-
 319 surface fresh layer tends to last longer in 2018 compared to 2019. The maximum near-surface
 320 salinity above 34.5 appears in SON. During the freshening periods, two waters with contrasting
 321 salinities in the vertical are becoming visible. The separation is between the near-surface low-
 322 salinity water and subsurface high-salinity water that sits below 70 m depth, indicating a strong
 323 salinity stratification in the Banda Sea that coincides with a relatively shallow MLD (> 25 m). It
 324 shall be noted that a shoaling of the MLD is also visible during the salinization events in SON.
 325 The upper-layer freshening is suspected to be linked to the eastward advection of JSW into the
 326 Banda Sea. Further, seasonal temperature and salinity profiles from Argo floats reveal that the
 327 ILD is almost always deeper than the MLD, indicating the appearance of seasonal barrier layers.

328



329

330 **Figure 5.** Time series of upper 200 m of (a, b, c) temperature ($^{\circ}\text{C}$) and (d, e, f) salinity in the
 331 Banda Sea from Argo 6901746 (left panel), Argo 5904961 (middle panel), and Argo 6901747

332 (right panel). Gray lines in **a, b, c** (**d, e, f**) show the ILD (MLD), while black lines in **d, e, f**
333 represent the BLT.

334

335 The BLT from Argo 6901746 shows seasonality with a bimodal distribution (Fig. 5d).
336 The barrier layer reaches the first maxima of more than 60 m depth in February-April. It attains
337 the second maxima (< 40 m) in June-July. However, the thickened barrier layer in February-
338 April is highly variable and sporadic, which appears to be linked to the local rainfall pattern in
339 the eastern Banda Sea. A recent study by Ismail et al. (2023) shows that there is increased
340 atmospheric convection from February to April, corresponding with a significant rise in
341 precipitation. The thickened barrier layer in June-July is more of a classical deepening picture
342 with less variability in time series. Because of the shorter time series (roughly one year), the BLT
343 from Argo 5904961 and 6901747 only show one peak in June-July (Fig. 5e) and March-April
344 (Fig. 5f), respectively and this synchronized with Argo 6901746 two-year record. It is worth
345 noting that the thick barrier layer reaches about 64 m in June-July, only captured by Argo
346 5904961 circling in the central/western Banda Sea (Fig. 1c), suggesting that the barrier layer
347 occurs in the western-central Banda Sea. The strong signal that originates from the JSW
348 advection is not fully captured by Argo 6901746 operating in the eastern Banda Sea, and thus the
349 BLT maximum in JJA is limited in vertical extent. Similarly, Argo 6901747's operating for about
350 8 to 9 months and covering only during SON to MAM. The BLT maximum in JJA mainly
351 reflects that of the ILD (Fig. 5a and 5b). Less than 10 m of barrier layer were observed from
352 Argo 5904961 and 6901746 found during SON in 2018 and 2019. Overall, the occurrence rates
353 of barrier layer (> 2 m) have been identified for almost all profiles of Argo 5904961, with a
354 mean value of 13.42 m. The occurrence rates of BLT from Argo 6901746 and Argo 6901747 are
355 about 90 % (Table 1), and have a mean thickness value ranging from 9.17 m to 9.67 m.

356

357 3.2 Barrier layer mean conditions

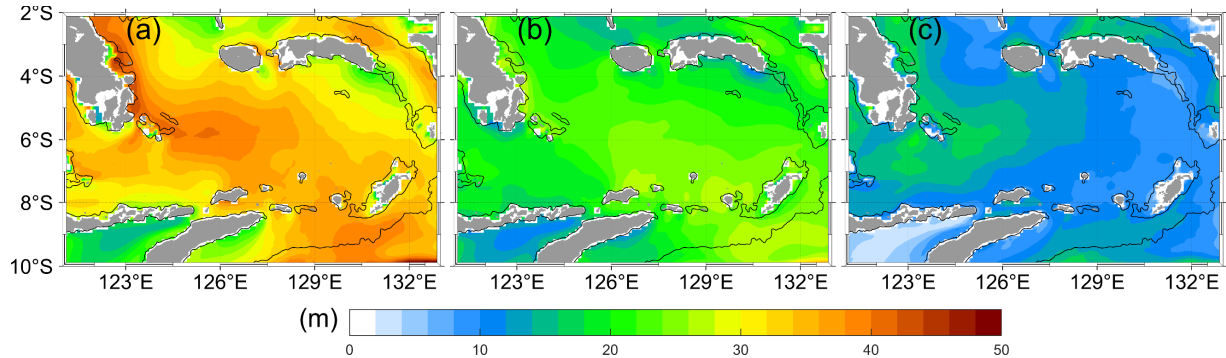
358 In order to set the variability into a context, we derived mean conditions of ILD, MLD,
359 and BLT (Fig. 6 and 7) from the BRAN2020 reanalysis product. The mean ILD distribution (Fig.
360 6a) is deeper than 30 m over a large part of the Banda Sea. A band of maximum ILD core with
361 values close to 50 m is found in the midwest of the Banda Sea, extending from the 5°S to 7°S
362 latitude and 125°E to 128°E longitude, as well as north-westward along the west boundary of
363 Lifamatola Passage. The mean MLD distribution is mainly shallower than the ILD and ranges
364 from about 16 m to 28 m (Fig. 6b). The spatial patterns of ILD and MLD exhibit significant
365 differences in value. The shallower MLD and deeper ILD indicate the presence of thick barrier
366 layers, as demonstrated in Fig. 6c. The mean BLT spatial structure clearly shows a band of BLT
367 deeper than 20 m observed along a path similar to the ILD maximum. The BLT maximum
368 appears to be located in the western region of the Banda Sea and centered around 5° - 7°S and
369 124° - 126°E . In contrast, BLT shallower than 10 m is mainly contained east of the Banda Sea.
370 The annual mean analysis provides a preferential region of the thicker BL in the Banda Sea.

371

372 The monthly evolution of BLT (Fig. 7) exhibits seasonal variation with distinct spatial
373 structures. Spatial characteristics of BLT distribution deeper than 10 m are generally along the

374 northern half of the Banda Sea between February and March/April. In addition, a band of
 375 shallower BLT (< 10 m) is observed along the southern half of the Banda Sea. By May, the
 376 region of barrier layers formed in the northern half of the Banda Sea builds up both in thickness
 377 and spatial extent southward.

378



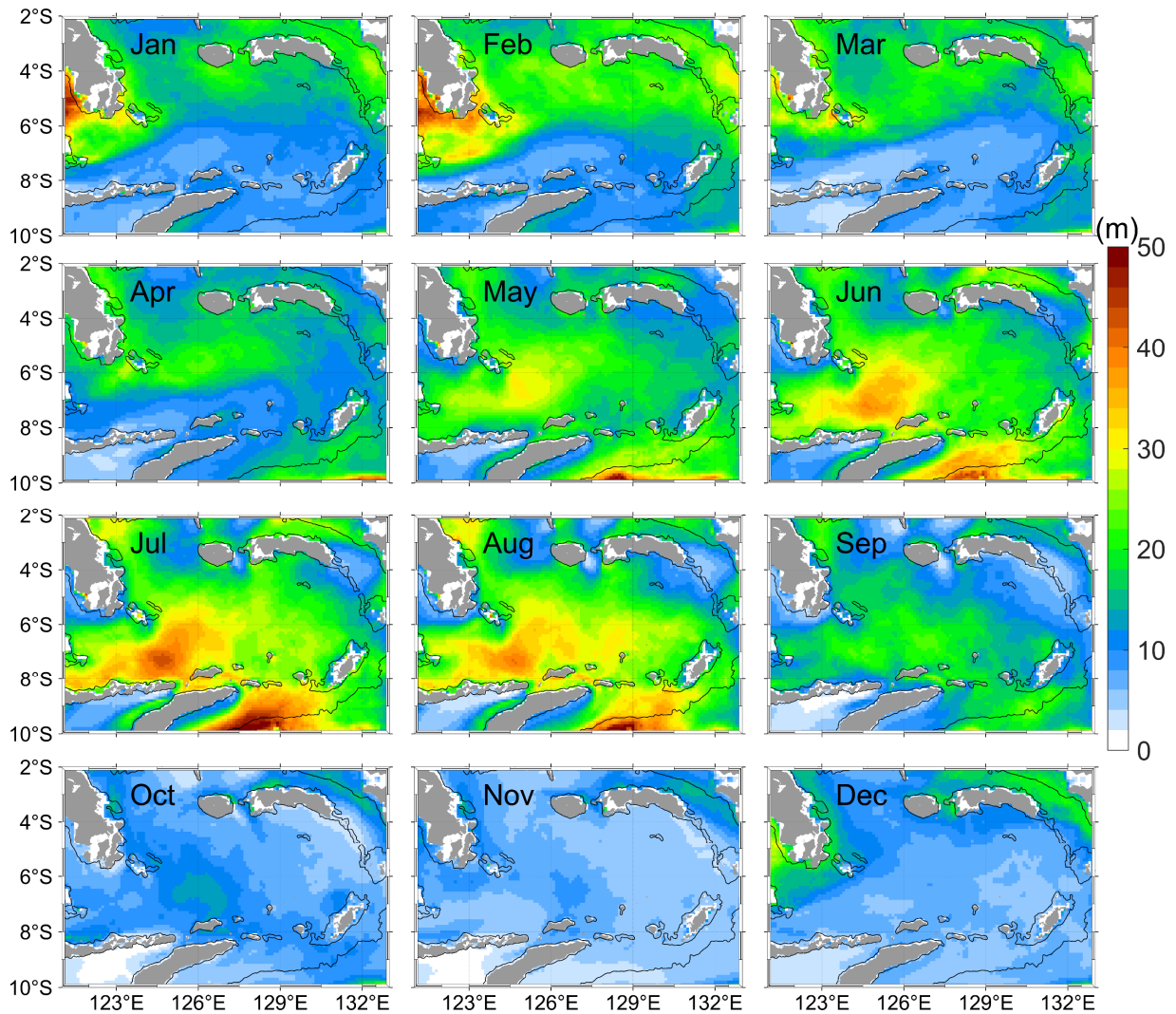
379

380 **Figure 6.** Climatological annual mean of (a) ILL, (b) MLD, and (c) BLT from 1993 to 2022.
 381 Black lines in a, b, and c represent the 500 m isobath. The ILL, MLD, and BLT are computed
 382 from the gridded product of BRAN2020 datasets.

383

384 During the JJA, the spatial distribution of BLT displays a noticeably different pattern
 385 from that of the DJF and MAM. The thick barrier layers (> 20 m) covered almost the entire
 386 Banda Sea during this period. It is observed that the BLT attains its seasonal maximum in JJA
 387 and is over 40 m deep in the mid-west of the Banda Sea, which is consistent with the BLT
 388 maximum observed with Argo 5904961 (Fig. 5e). This region of high BLT appears as a rather
 389 steady feature that has not been reported in the past. The region that encompasses the seasonal
 390 BLT maximum during JJA in Fig. 7 agrees with the pattern of the annual mean structure shown
 391 in Fig. 6c. This similarity suggests a significant contribution of BLT during the JJA to the annual
 392 mean field. With the beginning of the SON, the barrier layers undergo a weakening phase. Its
 393 spatial extent begins to decrease by September, albeit thick BLT (~ 20 m) still occurs in a large
 394 area spanning from the center to the west of the Banda Sea (Fig. 7). In October and November,
 395 the BLT mainly decreases to under 10 m with the thick barrier layers core centered around 6°S to
 396 8°S latitude and 124°E and 126°E longitude. The weakest BLT is observed in November and
 397 December, with its value generally not more than 10 m, and appears in a thin and patchy in the
 398 Banda Sea. The BLT formation can be summarized into four major stages: the initial stage
 399 during DJF, the development and peak stages in MAM and JJA, respectively, and the decaying
 400 stage in SON.

401



402

403 **Figure 7.** Monthly mean BLT (m) climatology in the Banda Sea based on BRAN2020 data from
 404 January 1993 to December 2022. Solid black lines represent the 500 m isobath.

405

406

3.3 Possible mechanism of the seasonal BLT variation

407

408

409

410

411

412

413

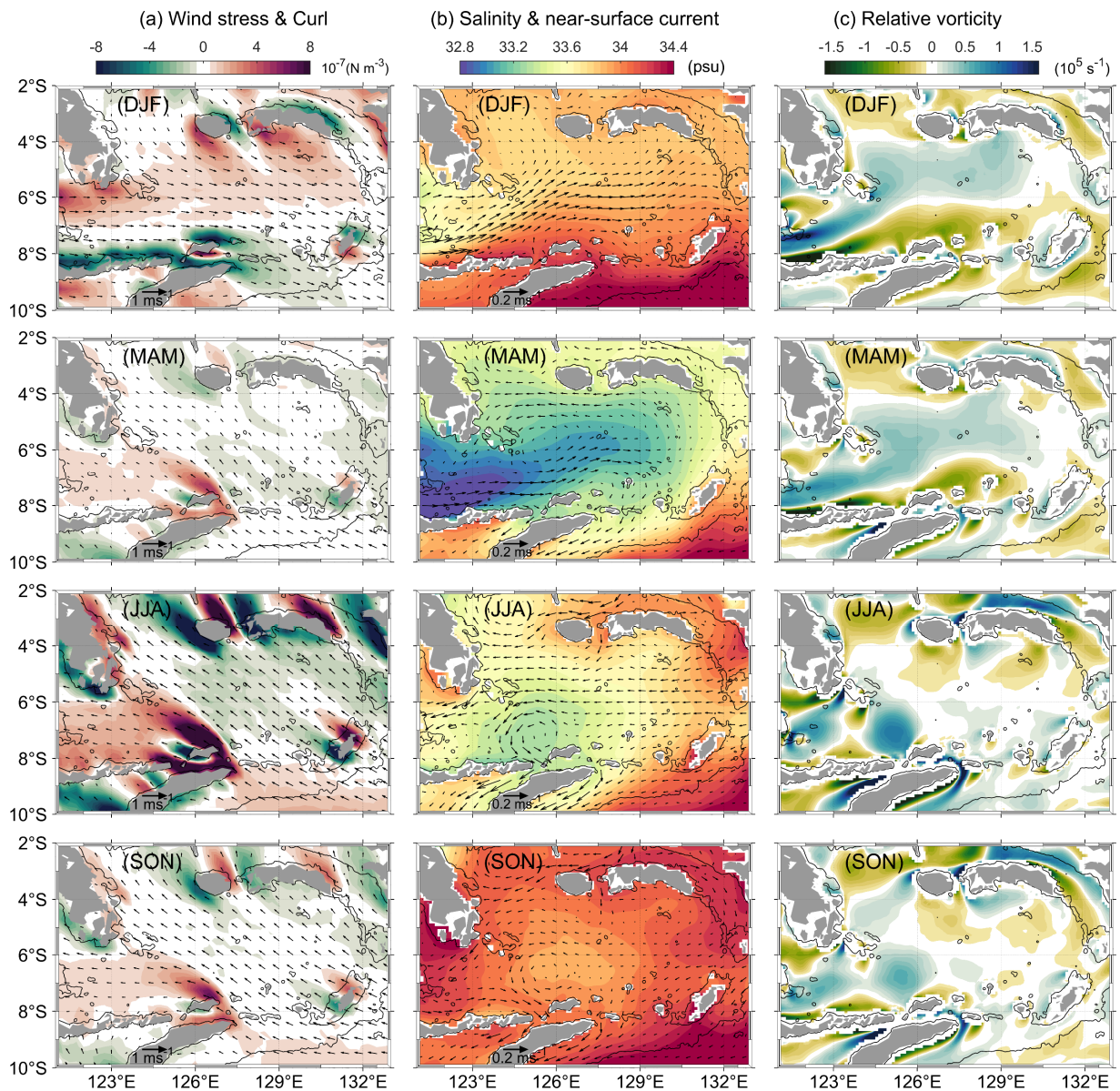
414

415

To understand the drivers of the seasonal BLT variation in the Banda Sea, we analyzed wind stress and wind stress curl, horizontal salinity advection, and mesoscale relative vorticity as a proxy for mesoscale activity. During DJF, the wind stress is northwesterly in the northern region of the Banda Sea and westerly in the south (Fig. 8a). Simultaneously, the surface circulation is in general northeast over the entire Banda Sea with the strongest current in the southwestern and central parts and weakest currents in the north (Fig. 8a). Westerly winds during the austral summer monsoon season create a positive curl north of about 7°S and a very strong negative curl at the southern boundary of the domain. From the north-eastward flow, a branch separates into eastward and northward flows at around 126°E longitude (Fig. 8b). From a surface

416 salinity point of view, the eastward flow can bring JSW into the Banda Sea. It is also responsible
 417 for the positive and negative relative vorticity due to the zonal shear in the flow field (Fig. 8c).
 418 The positive and negative relative vorticity establishes a near-surface double gyre circulation in
 419 the basin: an anticyclonic circulation in the northern and cyclonic circulation in the southern part
 420 of the Banda Sea that observed during DJF. A recent modelling study by Zhu et al. (2019) also
 421 reported this particular circulation pattern. In line with anticyclonic circulation in the northern
 422 half of the Banda Sea, a warm SST (Fig. 5) and an ILD deepening (Fig. 9a) are found.
 423 Meanwhile, the eastward advection of low salinity water from the Java Sea (JSW) supports a
 424 shoaling of the MLD (Fig. 9b). The difference between them begins to emerge, leading to a
 425 distinct BLT distribution in the north and the south of the Banda Sea (see Fig. 7).

426



427

428 **Figure 8.** Seasonal monthly climatology of (a) wind stress (vectors) overlaid with wind stress
 429 curl (10^{-7} N m^{-3}), (b) surface salinity overlaid with near-surface current (vectors) from
 430 BRAN2020, and (c) relative vorticity (10^5 s^{-1}) during the period of January 1993 to December
 431 2022 in the Banda Sea. The black contour lines represent the 500 m isobath. Wind stress and
 432 wind stress curl are computed using the ERA5 winds. Relative vorticity is calculated from
 433 BRAN2020.

434

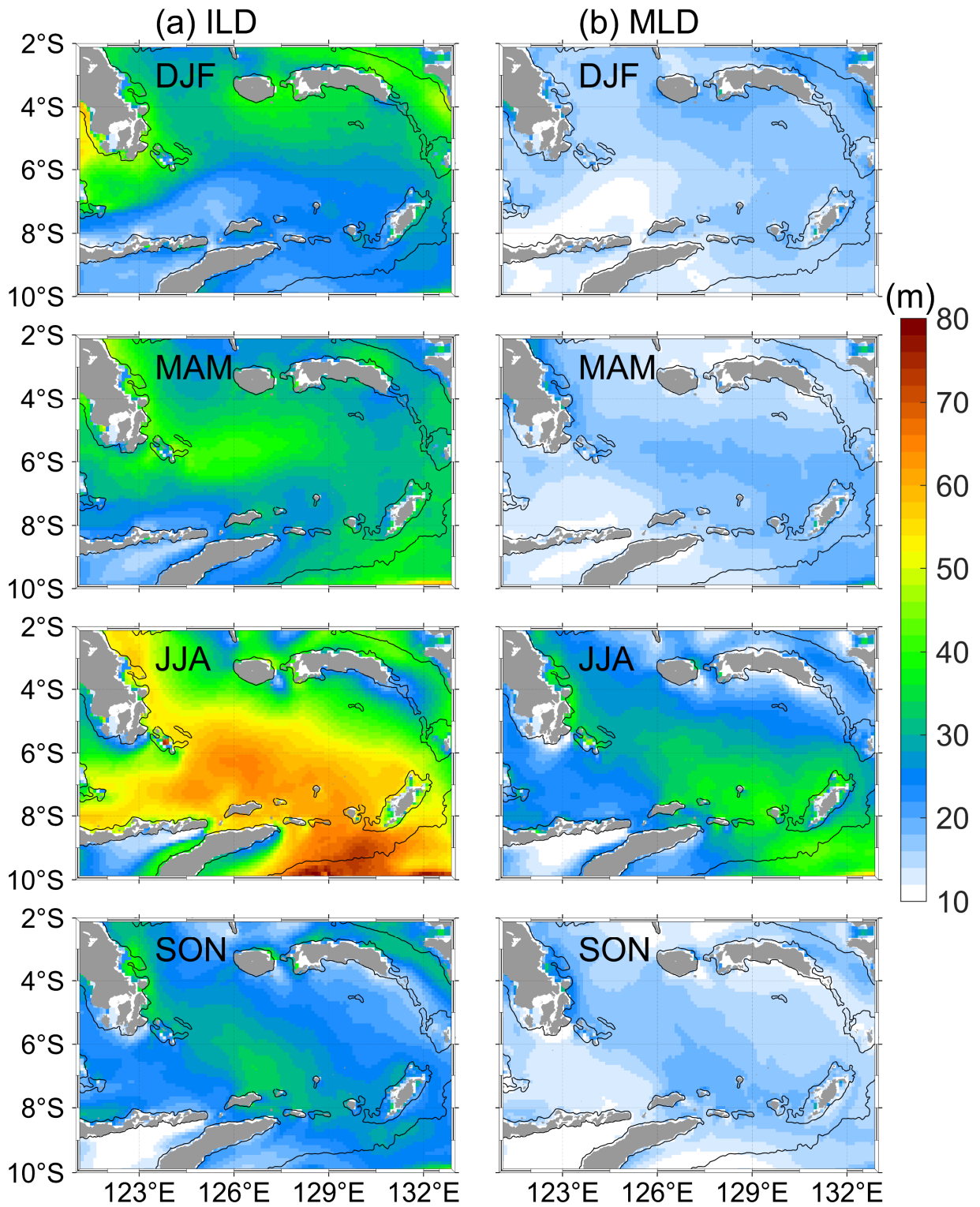
435 The spatial distribution of thicker BLT expands during the onset of southeasterly winds
 436 in MAM, consistent with the evolution of the ILD. The BLT deepening during this period is
 437 likely regulated by the freshening of the upper water column due to the further redistribution of
 438 JSW and supported by anticyclonic circulation. These can be manifested in the spatial
 439 distribution of the thickened BLT core (Fig. 7) that emulates freshening salinity events and
 440 widening positive relative vorticity, as shown in Fig. 8b and 8c. In addition, the deepened ILD
 441 (Fig. 9a) concurred with the dominated positive relative vorticity region (Fig. 8c). The presence
 442 of an anticyclonic circulation pattern during MAM likely corresponded with longer water
 443 retention, which influenced the ocean's upper layer dynamic (d'Ovidio et al., 2013) and
 444 contributed to the ILD deepening. The relatively weak southeasterly wind stress during monsoon
 445 transition drives a sluggish southwestward Ekman transport and slight wind-driven mixing
 446 (Halkides et al., 2011; Sprintall & Liu, 2005; Thomas et al., 2003) that could lead to the slight
 447 deepening of ILD and MLD. However, the presence of the low salinity of JSW over the high
 448 salinity water during MAM generates strong salinity stratification, which shoals the MLD that
 449 are relatively similar to those of DJF (Fig. 9b). This freshwater of JSW is trapped over the Banda
 450 Sea and spreads along the Timor Passage toward the eastern Indian Ocean (Kida et al., 2019),
 451 which can be seen in Fig. 8b. The significant role of low salinity water horizontal advection to
 452 the MLD was also observed by Halkides et al. (2011) and Ismail et al. (2023). The resultant ILD
 453 thickening and MLD shoaling then favor a deep barrier layer in the Banda Sea forced by a
 454 shallow MLD that limits the momentum input to the near-surface mixed layer only. Consistent
 455 with the zonal band of deep ILD, the thickened barrier layer occurs during MAM. Further, the
 456 filament of a thick barrier layer ($> 20 \text{ m}$) always appears in the low salinity region and positive
 457 relative vorticity distribution in the Banda Sea (Fig. 8b and 8c).

458

459 The physical mechanisms that lead to the peak phase of the BLT in the Banda Sea during
 460 JJA are explored. The thickened BLT distribution in JJA likely corresponds with the
 461 convergence of the Ekman transport estimated from the wind stress curl and robust positive
 462 relative vorticity, particularly on the central and western Banda Sea and low salinity water of
 463 JSW over the central basin (Kida et al., 2019). A very good coincidence exists between the BLT
 464 maximum ($\sim 50 \text{ m}$), as shown during JJA in Fig. 7, with positive wind stress curl, relatively low
 465 salinity water, and intense positive relative vorticity indicative of anticyclonic circulation cell
 466 centered in the 7°S latitude and 125°E longitude (Fig. 8). A possible explanation is that the
 467 Ekman transport convergence that supports the anticyclonic circulation cell also generates deeper
 468 ILD and MLD (see Fig. 9). During this time, the energetic wind stress curls induce Ekman
 469 downwelling (upwelling) primarily on the western (eastern) side of the Banda Sea (Gordon &
 470 Susanto, 2001; Thomas et al., 2003). While we expect that upwelling favors ILD and MLD

471 shallowing and vice versa, an early study by Gordon and Susanto (2001) in the Banda Sea during
472 JJA suggested that upwelling favorable wind was always associated with cooler near-surface
473 temperature but not always with shallower ILD. Using a mixed layer heat and salinity budget,
474 Halkides et al. (2011) argued that a strong southeast monsoon increases wind-driven vertical
475 diffusivity that causes ILD and MLD to deepen. However, Thomas et al. (2003) hypothesized
476 that the shallowing ILD and MLD are eroded by the intense southeasterly wind-induced mixing,
477 which also contributes to the ILD and MLD deepening (Fig. 9). Although both ILD and MLD
478 are deepening, ILD is always deeper than MLD, therefore dominating the thickening of barrier
479 layers spatial pattern in the Banda Sea during JJA.

480



481

482 **Figure 9.** Seasonal monthly climatology of **(a)** ILD (m) and **(b)** MLD (m) for the period of
 483 January 1993 to December 2022 in the Banda Sea. The 500 m isobaths are shown in black lines.
 484 ILD and MLD are calculated from BRAN2020.

485

486 The decaying phase of BLT in the Banda Sea during SON is in line with the changes in
 487 wind stress from southeasterly winds and an associated relaxation in the curl Ekman pumping,
 488 respectively. More saline waters appear at the surface, and also the surface ocean is affected by a
 489 net evaporation changing of salinity regime to salinization-dominated waters (Halkides et al.,
 490 2011; Ismail et al., 2023) and a remnant of positive relative vorticity in the same spot as in JJA.
 491 The characteristics of ILD and MLD spatial distribution are slightly similar to those of during
 492 MAM, except that their thickness is shallower. The presence of higher salinity surface water over
 493 the Banda Sea leads to weak stratification and a thick MLD. However, Halkides et al. (2011)
 494 suggested that the wind stress curl from the southeasterly winds will shoal the pycnocline, thus
 495 against the MLD deepening due to weak stratification. At the same time, the vertical temperature
 496 shows a weaker gradient than the vertical salinity due to higher net heat gain by the ocean, which
 497 favors a thickened ILD than MLD (Halkides et al., 2011; Ismail et al., 2023). The thickened
 498 barrier layer (~ 10m) during SON is restricted to the western side of the Banda Sea. It distributes
 499 symmetrically with the positive relative vorticity, suggesting the role of an anticyclonic gyre in
 500 maintaining deep ILD and modulating the BLT spatial distribution during SON.

501

502 **4 Summary and Conclusions**

503 The seasonal evolution of the Barrier Layer occurrence in the Banda Sea and the potential
 504 drivers for the seasonality have been analyzed. This way, we extend the study by Ismail et al.
 505 (2023), based on a single Argo float in the eastern Banda Sea, to the whole area. We use all the
 506 available in-situ CTD profile data and also consider ocean reanalysis model data BRAN2020. In
 507 the CTD data, barrier layers are identified for more than 90 % of profiles, with about 72 % with a
 508 thickness of less than 10 m. We also found a quasi-permanent barrier layer exists in the Banda
 509 Sea but with seasonal variations. The BLT maximum and minimum in the Banda Sea were
 510 identified in JJA and SON, respectively. Observations also displayed that thickened barrier
 511 layers in the Banda Sea concurred with the freshening events during MAM and early JJA. We
 512 have shown that these freshening events were caused by the eastward advection of low salinity
 513 JSW near the surface, which created a MLD shoaling.

514

515 The annual climatological mean distribution of BLT in BRAN2020 illustrated a hot spot
 516 of thicker barrier layers in the central/western region of the Banda Sea and centered around 6°-
 517 8°S and 124°-126°E. This pattern also is evident in the monthly mean fields. Our results suggest
 518 that the monthly climatological cycle of BLT can be divided into four stages according to its
 519 seasonal variation: the initial stage during DFJ, the development and peak stage in MAM and
 520 JJA, respectively, and the attenuation stage in SON. In its initial stage, the barrier layer forms
 521 when Ekman pumping and anticyclonic circulation increase and in turn deepen the ILD. On the
 522 contrary, the advection of low salinity surface water from the Java Sea (JSW) shoals the MLD.

523 The development period of BLT in MAM is mainly attributed to the near-surface water
524 freshening due to the presence of JSW that induces strong vertical salinity stratification, which
525 shoals the MLD and deep ILD maintained by enhanced anticyclonic gyre. The freshening events
526 during MAM provide a precondition for the development of shallower MLD in the following
527 months. The combination of energetic southeasterly wind, anticyclonic circulation cells, and
528 relatively low salinity water from JSW are more pronounced for the peak period of BLT in JJA.
529 The convergence zone due to wind stress curl-induced Ekman pumping and robust anticyclonic
530 circulation cells favor a deep ILD and MLD, albeit MLD deepening is limited by salinity
531 stratification. We found that strong southeasterly wind stress in JJA also contributes to deepening
532 the ILD and MLD through wind-driven mixing and vertical, upward mixing of higher salinity
533 subsurface water, as previously documented by Halkides et al. (2011) and Thomas et al. (2003).
534 During SON, the barrier layers are the thinnest of the year. Though their thickness is shallower,
535 the ILD and MLD spatial distributions are marginally comparable to those during the MAM. The
536 BLT is likely maintained by the southeasterly wind stress and curl corresponding with shoaled
537 the pycnocline and MLD and relatively thickened ILD related to the higher net heat gain by the
538 ocean as noted in Halkides et al. (2011) and Ismail et al. (2023).

539

540 Here, we provide a first description of the BLT seasonal cycle and identify the processes
541 that control the seasonal barrier layer's development and erosion in the Banda Sea. We
542 demonstrated the presence of a quasi-permanent anticyclonic circulation cell in the Banda Sea,
543 which might facilitate the retention of low-salinity surface water during MAM and JJA and thus
544 help to maintain a thick BLT and a shallow MLD, respectively. Given that the anticyclonic
545 circulation aligns with the regional Ekman pumping pattern, it is most likely driven by wind.
546 Modulation of the anticyclonic gyre is via seasonal variability in the wind stress curl, which may
547 explain the efficiency of freshwater retention. It thus helps maintain the BLT and make it more
548 coherent during JJA. The mechanisms responsible for the BLT variation discussed here can be
549 applied to subtropical and equatorial regions where mesoscale circulation patterns and
550 substantial freshwater influx are prevalent. The BLT has a notable impact on the SST.

551

552 This study's description of BLT and its seasonal variation may help understand the
553 ocean's role in air-sea interaction processes regulating substantial SST cooling in the Banda Sea
554 (Pei et al., 2021). It is worth emphasizing that the thickening of barrier layers off west Sumatra
555 relates to increased rainfall over northern Australia (Ivanova et al., 2021). We will explore this
556 potential link of the thermal impact of the barrier layer in the Banda Sea to the local rainfall over
557 the IMC in the future. The analysis presented in this work focuses mainly on the BLT's seasonal
558 change and annual mean state. It also is a study that shows that the BRAN2020 provides a very
559 good state description for the Banda Sea region. However, it is known that intraseasonal and
560 interannual oceanic and atmospheric variability in the Banda Sea is significant, arising from
561 tropical atmospheric phenomena such as MJO (Napitu et al., 2015) and large-scale climate of the
562 Indo-Pacific region, including IOD (Yoneyama & Zhang, 2020) and ENSO (Gordon & Susanto,
563 2001). In future work, we will investigate the quantitative analysis of the remote forcing
564 mechanisms driving BLT variability at intraseasonal and interannual time scales.

565

566 **Acknowledgments**

567 This work is funded by the Georg Foster Research Fellowship of the Alexander von Humboldt-
 568 Stiftung. MFAI acknowledges support from GEOMAR Helmholtz Centre for Ocean Research
 569 Kiel and the National Research and Innovation Agency of Indonesia (BRIN). The authors thank
 570 three anonymous reviewers for their constructive comments and suggestions.

571
572 **Open Research**573 **Data Availability Statement**

574 Argo data were compiled and made freely available by the International Argo Program and the
 575 national programs contributing to it (<http://www.argo.ucsd.edu>, <http://argo.jcommops.org>). The
 576 Argo Program is part of the Global Ocean Observing System of the Coriolis Data Assembly
 577 Center (<http://doi.org/10.17882/42182>). ODP2016 data are available upon request. WOD18 data,
 578 documentation and information can be found at <http://www.nodc.noaa.gov/OC5/indprod.html>.
 579 The BRAN2020 data are available at <https://doi.org/10.25914/6009627c7af03>. ERA5 data
 580 provided by the Copernicus Climate Change Service (C3S) Climate Data Store can be found at
 581 <https://doi.org/10.24381/cds.adbb2d47>.
 582

583 **References**

- 584 Atmadipoera, A. S., Koch-Larrouy, A., Madec, G., Grelet, J., Baurand, F., Jaya, I., & Dadou, I.
 585 (2022). Part I: Hydrological properties within the eastern Indonesian throughflow region
 586 during the INDOMIX experiment. *Deep Sea Research Part I: Oceanographic Research*
 587 *Papers*, 182, 103735.
- 588 Boyer, T., Baranova, O., Coleman, C., Garcia, H., Grodsky, A., Locarnini, R., et al. (2018).
 589 World Ocean Database 2018. NOAA Atlas NESDIS 87. *Mishonov, Technical Ed. Silver*
 590 *Spring, MD*.
- 591 Breugem, W.-P., Chang, P., Jang, C., Mignot, J., & Hazeleger, W. (2008). Barrier layers and
 592 tropical Atlantic SST biases in coupled GCMs. *Tellus A: Dynamic Meteorology and*
 593 *Oceanography*, 60(5), 885-897.
- 594 Chamberlain, M. A., Oke, P. R., Fiedler, R. A., Beggs, H. M., Brassington, G. B., & Divakaran,
 595 P. (2021). Next generation of Bluelink ocean reanalysis with multiscale data assimilation:
 596 BRAN2020. *Earth System Science Data*, 13(12), 5663-5688.
- 597 Corbett, C. M., Subrahmanyam, B., & Giese, B. S. (2017). A comparison of sea surface salinity
 598 in the equatorial Pacific Ocean during the 1997–1998, 2012–2013, and 2014–2015 ENSO
 599 events. *Climate Dynamics*, 49(9), 3513-3526.
- 600 d’Ovidio, F., De Monte, S., Della Penna, A., Cotté, C., & Guinet, C. (2013). Ecological
 601 implications of eddy retention in the open ocean: a Lagrangian approach. *Journal of*
 602 *Physics A: Mathematical and Theoretical*, 46(25), 254023.
- 603 de Boyer Montégut, C., Madec, G., Fischer, A. S., Lazar, A., & Iudicone, D. (2004). Mixed layer
 604 depth over the global ocean: An examination of profile data and a profile-based
 605 climatology. *Journal of Geophysical Research: Oceans*, 109(C12).

- 606 de Boyer Montégut, C., Mignot, J., Lazar, A., & Cravatte, S. (2007). Control of salinity on the
607 mixed layer depth in the world ocean: 1. General description. *Journal of Geophysical*
608 *Research: Oceans*, 112(C6).
- 609 Drushka, K., Sprintall, J., & Gille, S. T. (2014). Subseasonal variations in salinity and barrier-
610 layer thickness in the eastern equatorial Indian Ocean. *Journal of Geophysical Research:*
611 *Oceans*, 119(2), 805-823.
- 612 Felton, C. S., Subrahmanyam, B., Murty, V. S. N., & Shriver, J. F. (2014). Estimation of the
613 barrier layer thickness in the Indian Ocean using Aquarius Salinity. *Journal of*
614 *Geophysical Research: Oceans*, 119(7), 4200-4213.
- 615 George, J. V., Vinayachandran, P. N., Vijith, V., Thushara, V., Nayak, A. A., Pargaonkar, S. M.,
616 et al. (2019). Mechanisms of Barrier Layer Formation and Erosion from In Situ
617 Observations in the Bay of Bengal. *Journal of Physical Oceanography*, 49(5), 1183-
618 1200.
- 619 Gordon, A. L., Ffield, A., & Ilahude, A. G. (1994). Thermocline of the Flores and Banda seas.
620 *Journal of Geophysical Research: Oceans*, 99(C9), 18235-18242.
- 621 Gordon, A. L., & Susanto, R. D. (2001). Banda Sea surface-layer divergence. *Ocean Dynamics*,
622 52(1), 2-10.
- 623 Halkides, D., Lee, T., & Kida, S. (2011). Mechanisms controlling the seasonal mixed-layer
624 temperature and salinity of the Indonesian seas. *Ocean Dynamics*, 61(4), 481-495.
- 625 Hersbach, H., Bell, B., Berrisford, P., Biavati, G., Horányi, A., Muñoz Sabater, J., et al. (2023).
626 ERA5 hourly data on single levels from 1979 to present. *Copernicus climate change*
627 *service (c3s) climate data store (cds)*, 10(10.24381).
- 628 Holte, J., & Talley, L. (2009). A new algorithm for finding mixed layer depths with applications
629 to Argo data and Subantarctic Mode Water formation. *Journal of Atmospheric and*
630 *Oceanic Technology*, 26(9), 1920-1939.
- 631 Ilahude, A. G., & Gordon, A. L. (1996). Thermocline stratification within the Indonesian Seas.
632 *Journal of Geophysical Research: Oceans*, 101(C5), 12401-12409.
- 633 Ismail, M. F. A., Karstensen, J., Ribbe, J., Arifin, T., Chandra, H., Akhwady, R., et al. (2023).
634 Seasonal mixed layer temperature and salt balances in the Banda Sea observed by an
635 Argo float. *Geoscience Letters*, 10(1), 1-9.
- 636 Ismail, M. F. A., Ribbe, J., Karstensen, J., Lemckert, C., Lee, S., & Gustafson, J. (2017). The
637 Fraser Gyre: A cyclonic eddy off the coast of eastern Australia. *Estuarine, Coastal and*
638 *Shelf Science*, 192, 72-85.
- 639 Ivanova, D. P., McClean, J. L., Sprintall, J., & Chen, R. (2021). The oceanic barrier layer in the
640 eastern Indian Ocean as a predictor for rainfall over Indonesia and Australia. *Geophysical*
641 *Research Letters*, 48(22), e2021GL094519.
- 642 Jochum, M., & Potemra, J. (2008). Sensitivity of tropical rainfall to Banda Sea diffusivity in the
643 Community Climate System Model. *Journal of Climate*, 21(23), 6445-6454.
- 644 Kara, A. B., Rochford, P. A., & Hurlburt, H. E. (2003). Mixed layer depth variability over the
645 global ocean. *Journal of Geophysical Research: Oceans*, 108(C3).
- 646 Katsura, S., Sprintall, J., Farrar, J. T., Zhang, D., & Cronin, M. F. (2022). The Barrier Layer
647 Effect on the Heat and Freshwater Balance from Moored Observations in the Eastern
648 Pacific Fresh Pool. *Journal of Physical Oceanography*, 52(8), 1705-1730.
- 649 Kida, S., Richards, K. J., & Sasaki, H. (2019). The Fate of Surface Freshwater Entering the
650 Indonesian Seas. *Journal of Geophysical Research: Oceans*, 124(5), 3228-3245.

- 651 Kumari, A., Kumar, S. P., & Chakraborty, A. (2018). Seasonal and interannual variability in the
 652 barrier layer of the Bay of Bengal. *Journal of Geophysical Research: Oceans*, *123*(2),
 653 1001-1015.
- 654 Lee, T., Fournier, S., Gordon, A. L., & Sprintall, J. (2019). Maritime Continent water cycle
 655 regulates low-latitude chokepoint of global ocean circulation. *Nature Communications*,
 656 *10*(1), 2103.
- 657 Li, Y., Han, W., Wang, W., Ravichandran, M., Lee, T., & Shinoda, T. (2017). Bay of Bengal
 658 salinity stratification and Indian summer monsoon intraseasonal oscillation: 2. Impact on
 659 SST and convection. *Journal of Geophysical Research: Oceans*, *122*(5), 4312-4328.
- 660 Liang, L., Xue, H., & Shu, Y. (2019). The Indonesian Throughflow and the Circulation in the
 661 Banda Sea: A Modeling Study. *Journal of Geophysical Research: Oceans*, *124*(5), 3089-
 662 3106.
- 663 Liang, Z., Xie, Q., Zeng, L., & Wang, D. (2018). Role of wind forcing and eddy activity in the
 664 intraseasonal variability of the barrier layer in the South China Sea. *Ocean Dynamics*,
 665 *68*(3), 363-375.
- 666 Lukas, R., & Lindstrom, E. (1991). The mixed layer of the western equatorial Pacific Ocean.
 667 *Journal of Geophysical Research: Oceans*, *96*(S01), 3343-3357.
- 668 Maes, C., Picaut, J., & Belamari, S. (2005). Importance of the Salinity Barrier Layer for the
 669 Buildup of El Niño. *Journal of Climate*, *18*(1), 104-118.
- 670 Mignot, J., de Boyer Montégut, C., Lazar, A., & Cravatte, S. (2007). Control of salinity on the
 671 mixed layer depth in the world ocean: 2. Tropical areas. *Journal of Geophysical*
 672 *Research: Oceans*, *112*(C10).
- 673 Napitu, A. M., Gordon, A. L., & Pujiana, K. (2015). Intraseasonal Sea Surface Temperature
 674 Variability across the Indonesian Seas. *Journal of Climate*, *28*(22), 8710-8727.
 675 <https://journals.ametsoc.org/view/journals/clim/28/22/jcli-d-14-00758.1.xml>
- 676 Oke, P. R., Griffin, D. A., Schiller, A., Matear, R., Fiedler, R., Mansbridge, J., et al. (2013).
 677 Evaluation of a near-global eddy-resolving ocean model. *Geoscientific model*
 678 *development*, *6*(3), 591-615.
- 679 Pang, S., Wang, X., Liu, H., Zhou, G., & Fan, K. (2019). Decadal variability of the barrier layer
 680 and forcing mechanism in the Bay of Bengal. *Journal of Geophysical Research: Oceans*,
 681 *124*(7), 5289-5307.
- 682 Pei, S., Shinoda, T., Steffen, J., & Seo, H. (2021). Substantial Sea Surface Temperature Cooling
 683 in the Banda Sea Associated With the Madden-Julian Oscillation in the Boreal Winter of
 684 2015. *Journal of Geophysical Research: Oceans*, *126*(6), e2021JC017226.
 685 <https://agupubs.onlinelibrary.wiley.com/doi/abs/10.1029/2021JC017226>
- 686 Pujiana, K., & McPhaden, M. J. (2018). Ocean Surface Layer Response to Convectively Coupled
 687 Kelvin Waves in the Eastern Equatorial Indian Ocean. *Journal of Geophysical Research:*
 688 *Oceans*, *123*(8), 5727-5741.
- 689 Qiu, Y., Cai, W., Li, L., & Guo, X. (2012). Argo profiles variability of barrier layer in the
 690 tropical Indian Ocean and its relationship with the Indian Ocean Dipole. *Geophysical*
 691 *Research Letters*, *39*(8).
- 692 Qu, T., & Meyers, G. (2005). Seasonal variation of barrier layer in the southeastern tropical
 693 Indian Ocean. *Journal of Geophysical Research: Oceans*, *110*(C11).
- 694 Rudnick, D. L., Zeiden, K. L., Ou, C. Y., Johnston, T. S., MacKinnon, J. A., Alford, M. H., &
 695 Voet, G. (2019). Understanding vorticity. *Oceanography*, *32*(4), 66-73.

- 696 Russo, C. S., Veitch, J., Carr, M., Fearon, G., & Whittle, C. (2022). An intercomparison of
697 global reanalysis products for Southern Africa's major oceanographic features. *Frontiers*
698 *in Marine Science*, 9, 284.
- 699 Schiller, A., Brassington, G. B., Oke, P., Cahill, M., Divakaran, P., Entel, M., et al. (2020).
700 Bluelink ocean forecasting Australia: 15 years of operational ocean service delivery with
701 societal, economic and environmental benefits. *Journal of Operational Oceanography*,
702 13(1), 1-18.
- 703 Schiller, A., Wijffels, S., Sprintall, J., Molcard, R., & Oke, P. R. (2010). Pathways of
704 intraseasonal variability in the Indonesian Throughflow region. *Dynamics of atmospheres*
705 *and oceans*, 50(2), 174-200.
- 706 Sprintall, J., & Liu, W. T. (2005). Ekman mass and heat transport. *Oceanography*, 18(4), 88.
- 707 Sprintall, J., & Tomczak, M. (1992). Evidence of the barrier layer in the surface layer of the
708 tropics. *Journal of Geophysical Research: Oceans*, 97(C5), 7305-7316.
- 709 Thadathil, P., Thoppil, P., Rao, R. R., Muraleedharan, P. M., Somayajulu, Y. K., Gopalakrishna,
710 V. V., et al. (2008). Seasonal Variability of the Observed Barrier Layer in the Arabian
711 Sea. *Journal of Physical Oceanography*, 38(3), 624-638.
- 712 Thomas, M., II, John, M., & Ali, A. (2003). Response of the Banda Sea to the southeast
713 monsoon. *Marine Ecology Progress Series*, 261, 41-49. [https://www.int-](https://www.int-res.com/abstracts/meps/v261/p41-49/)
714 [res.com/abstracts/meps/v261/p41-49/](https://www.int-res.com/abstracts/meps/v261/p41-49/)
- 715 Wang, Z., Yin, X., Li, X., Li, Y., Li, R., Yang, Y., et al. (2023). Water Mass Variations in the
716 Maluku Channel of the Indonesian Seas During the Winter of 2018–2019. *Journal of*
717 *Geophysical Research: Oceans*, 128(3), e2022JC018731.
- 718 Wong, A. P. S., Wijffels, S. E., Riser, S. C., Pouliquen, S., Hosoda, S., Roemmich, D., et al.
719 (2020). Argo Data 1999–2019: Two Million Temperature-Salinity Profiles and
720 Subsurface Velocity Observations From a Global Array of Profiling Floats. *Frontiers in*
721 *Marine Science*, 7. Systematic Review.
- 722 Yin, X., Yuan, D., Li, X., Wang, Z., Li, Y., Corvianawatie, C., et al. (2023). Moored
723 Observations of the Currents and Transports of the Maluku Sea. *Journal of Physical*
724 *Oceanography*, 53(1), 3-18.
- 725 Yoneyama, K., & Zhang, C. (2020). Years of the Maritime Continent. *Geophysical Research*
726 *Letters*, 47(12), e2020GL087182.
- 727 Yuan, D., Yin, X., Li, X., Corvianawatie, C., Wang, Z., Li, Y., et al. (2022). A Maluku Sea
728 intermediate western boundary current connecting Pacific Ocean circulation to the
729 Indonesian Throughflow. *Nature Communications*, 13(1), 2093.
- 730 Zhu, Y., Wang, L., Wang, Y., Xu, T., Li, S., Cao, G., et al. (2019). Stratified Circulation in the
731 Banda Sea and Its Causal Mechanism. *Journal of Geophysical Research: Oceans*,
732 124(10), 7030-7045.

733
734